ATL-PHYS-2003-037

Study of Black Holes with the ATLAS detector at the LHC

J. Tanaka[1,†], T. Yamamura[2], S. Asai[1], J. Kanzaki[3]

[1] International Center for Elementary Particle Physics (ICEPP), University of Tokyo
[2] Department of Physics, Faculty of Science, University of Tokyo
[3] High Energy Accelerator Research Organization (KEK)
[†] Mail address: Junichi.Tanaka@cern.ch

Abstract

We evaluate the potential of the ATLAS detector for discovering black holes produced at the LHC, as predicted in models with large extra dimensions where quantum gravity is at the TeV scale. We assume that black holes decay by Hawking evaporation to all Standard Model particles democratically. We comment on the possibility to estimate the Planck scale.

1 Introduction

Black holes will be produced at the Large Hadron Collider (LHC) if the fundamental Planck scale is of order a TeV [1, 2]. This scenario occurs in the model of large extra dimensions [3] proposed by Arkani-Hamed, Dimopoulos and Dvali, where the Standard Model (SM) gauge and matter fields are confined to a 3-dimensional brane while gravity is free to propagate in extra dimensions of large size. This model was motivated by the necessity to solve the hierarchy problem.

Using Gauss' law, the fundamental Planck scale of the $(4+n)$-dimension M_P is related to the 4-dimensional Planck scale $M_{\rm Pl}$ ($\sim 10^{19}$ GeV) by

$$M_{\rm Pl}^2 \sim M_P^{n+2} R^n,$$

where n is the number of extra dimensions and R is the size of the compactified dimensions. Assuming that the fundamental Planck scale M_P is the same as the electroweak scale ($\sim$1 TeV), the case $n = 1$ yields a very large R ($\sim 10^{13}$ cm), ruled out by experiments. For $n \geq 2$, the size of R is less than $\sim 10^{-2}$ cm, which does not contradict results of gravitational experiments [4]. From astrophysical constraints [5], the size of M_P is larger than O(TeV) and O(10 TeV) for $n = 2$ and 3, respectively. In particular, the case of $n = 2$ would be ruled out from the point of view of the solution of the hierarchy problem [6].

We consider here black holes of mass $M_{\rm BH}$ much larger than the fundamental Planck scale M_P since the phenomenology of black holes at $M_{\rm BH} \sim M_P$ is very complex and beyond the scope of the present study.

For the collision of two partons at a center-of-mass energy $\sqrt{\hat{s}} = M_{\rm BH}$, by classical arguments [1] the total cross section is given by

$$\sigma(M_{\rm BH}) \sim \pi R_{\rm S}^2 = \frac{1}{M_P^2}[\frac{M_{\rm BH}}{M_P}(\frac{8\Gamma(\frac{n+3}{2})}{n+2})]^{\frac{2}{1+n}},$$

where $R_{\rm S}$ is the Schwarzschild radius:

$$R_{\rm S} = \frac{1}{\sqrt{\pi} M_P}[\frac{M_{\rm BH}}{M_P}(\frac{8\Gamma(\frac{n+3}{2})}{n+2})]^{\frac{1}{1+n}}.$$

For proton-proton collisions at the LHC, the differential cross section is given by

$$\frac{d\sigma(pp \to {\rm BH} + X)}{dM_{\rm BH}} = \frac{dL}{dM_{\rm BH}} \hat{\sigma}(ab \to {\rm BH})|_{\hat{s}=M_{\rm BH}^2}, \tag{1}$$

$$\frac{dL}{dM_{\rm BH}} = \frac{2M_{\rm BH}}{s} \sum_{a,b} \int_{M_{\rm BH}^2/s}^1 \frac{dx_a}{x_a} f_a(x_a) f_b(\frac{M_{\rm BH}^2}{s x_a})$$

$$\hat{\sigma}(ab \to {\rm BH})|_{\hat{s}=M_{\rm BH}^2} = \pi R_{\rm S}^2,$$

where a and b are partons in protons and $f_i(x)$ are the parton distribution functions (PDFs). An exponential suppression of the geometrical cross section has been proposed by Voloshin [7]. However since subsequent studies did not support this result [8], we do not consider the effect here.

Black holes decay through several phases [2]: *balding*, *Hawking evaporation* (*spin-down* and *Schwarzschild*) and *Planck* phases. Since the *Hawking evaporation* phase is expected to be the main phase of the decay, we naively consider only this process and assume that a black hole evaporates until its mass becomes zero.

The radiation is characterized by the Hawking temperature T_H,

$$T_H(M_P, n, M_{\rm BH}) = M_P\left(\frac{M_P}{M_{\rm BH}}\frac{n+2}{8\Gamma(\frac{n+3}{2})}\right)^{\frac{1}{n+1}}\frac{n+1}{4\sqrt{\pi}} = \frac{n+1}{4\pi R_{\rm S}}.$$

The heavier the black hole, the colder are its decay products. As it evaporates, its temperature increases but we will ignore the time evolution of black holes in this phase.

We assume that the evaporation is described by black body radiation. The energy spectrum of the decay products obeys the Boltzmann distribution [1]:

$$\frac{dN}{dE} \sim \frac{x^2}{e^x + c},$$

where $x \equiv E/T_H$ and c is a constant, which depends on the quantum statistics of the decay products, i.e., $c = -1, +1, 0$ for bosons, fermions and Boltzmann statistics, respectively. In this study, we use $c = 0$ for all particles.

Certain conservation laws are obeyed in the decay of back holes. We assume that black holes decay "democratically", i.e., with roughly equal probability to all of the SM particles.

In this paper, we present the discovery potential of the black holes at the LHC. We describe a method of estimation of the fundamental Planck scale M_P from the discovery potential.

The outline of this paper is as follows: the simulation conditions and description of signal and background samples are given in Section 2. Our original generator of the black holes is explained in detail in Section 3. In Section 4, we describe the event selection and the reconstruction and finally, a conclusion is given in Section 5.

2 Simulation

The generator, developed for the purpose of this study, is described in Section 3. Initial state parton showers, hadronisation and decay are performed using PYTHIA 6.2 [9]. All background samples are generated by PYTHIA 6.2. CTEQ5L is used for the parton distribution function.

All samples are processed through the parameterized simulator, ATLFAST [10], of the ATLAS detector. The energy resolutions and efficiencies for jet and particle reconstruction are corrected using the results of the full detector simulation.

2.1 Signal

We have generated signal samples for the various values of (M_P, n) listed in Table 1. We have generated black holes whose mass $M_{\rm BH}$ is larger than M_P. Factorization and renormalization scales are set to a mass $M_{\rm BH}$ of the generated black hole. We call the lower limit of a black hole mass a threshold mass $M_{\rm BH}^{\rm th} = f_{\rm BH}^{\rm th} \times M_P$. We assume that

the energy spectrum of all the products from the black hole decay obeys the Boltzmann distribution.

Table 1: Cross section of signal samples for each (M_P, n) parameter. $f_{\rm BH}^{\rm th}$, which is described in the text, is 1 for all cases. The unit of M_P is TeV.

M_P, n	σ (pb)	M_P, n	σ (pb)
1,2	$9.45 \cdot 10^3$	5,2	0.662
1,3	$8.26 \cdot 10^3$	5,3	0.603
1,4	$8.06 \cdot 10^3$	5,5	0.625
1,5	$8.24 \cdot 10^3$	5,7	0.699
1,7	$9.05 \cdot 10^3$		
3,2	25.5	6,2	0.125
3,3	22.9	6,3	0.114
3,5	23.4	6,5	0.119
3,7	26.0	6,7	0.133
4,2	3.74	7,2	0.0229
4,3	3.38	7,3	0.0210
4,5	3.49	7,5	0.0220
4,7	3.89	7,7	0.0247

2.2 Background

Our background samples are listed in Table 2. We use kinematical cuts at generation level to save CPU time and storage space of the data. The lower limit for the energy in the center-of-mass of initial partons, is set to 50 GeV for all the samples. The lower limit for the transverse momentum in the rest frame of initial partons $\hat{p}_T^{min}$, is also used as shown in Table 2.

Table 2: Cross section of background samples for each mode. "Proc" is a process identification defined in the PYTHIA.

Process	σ (pb)	$\hat{p}_T^{min}$	Proc
qq (q =quark,lepton,gluon)	$1.29 \cdot 10^4$	280.0	11,12,13,28,53,68
$t\bar{t}$	493	10.0	81,82
$W^{\pm}W^{\mp}$	0.468	240.0	25
$W^{\pm}Z$	25.9	10.0	23
ZZ	10.6	10.0	22
$\gamma\gamma$	229	10.0	18,114
γV ($V = W^{\pm}, \gamma^*, Z$)	280	10.0	19,20
$W^{\pm}q$	73.4	240.0	16,31
Zq,γ^*q	31.5	240.0	15,30
γq	23.5	240.0	14,29,115

3 Generator

A black hole generator was developed for this study, based on the assumptions and approximations discussed in Section 1[1].

We require the following conditions for the decay of black holes:

- The number of fermions constrained by spin conservation
- Four-Momentum conservation
- Assumption of Boltzmann distribution for the energy spectrum of decay products
- Color conservation
- Assumption of democratic decay
- Charge conservation
- Option of conservation of the difference between the lepton number and the baryon number ($B - L$ conservation)
- Option of implementing Voloshin suppression [7]

We can select whether to apply the $B - L$ conservation and the Voloshin suppression, but they are switched off (no $B - L$ conservation and no Voloshin suppression) in this study.

For the production of the black holes, we use the Eq. (1) of Section 1. Using the PDFs, the types of partons in the initial hard scattering are selected randomly.

3.1 Spin Conservation

We require that the number of fermions in the decay products of the black holes be even or odd according to the parity of the number of initial state fermions. Note that we do not consider gravitons in this study.

3.2 Four-Momentum Conservation and Boltzmann Distribution

We assume that the energy spectrum of the decay products follows a Boltzmann distribution. However, since energy and momentum must be conserved, all particles cannot be sampled randomly from that distribution. We do not allow the case $N = 2$ since it is fully constrained. For $N \geq 3$, particle energies are successively sampled from the Boltzmann distribution until the summed energy exceeds the mass of the black hole. The last particle is then given the energy required by the energy constraint. The first $N - 2$ particles are assigned random directions and the last two are emitted in a direction such as to conserve overall momentum.

[1]Assumptions and approximations of our generator are similar with a generator, TRUENOIR, described in [11]. Another generator has recently been published [12].

3.3 Color Conservation

Color is assumed conserved in the decay of black holes. Color is assigned to the initial partons and color connection is implemented. As an example, if the initial partons are two gluons, we select randomly either a $q\bar{q}$ pair or a gluon from the final state partons, if present. We then connect the colors as shown in Figure 1. If no $q\bar{q}$ pair or gluon is present, the color connection must be applied between the two initial state gluons, if possible. Another example of color connection when the initial partons are a quark and a gluon is shown in Figure 1.

For the remaining partons, color connection is applied between pairs with closest opening angle. If there is an odd gluon remaining, it is connected to the $q\bar{q}$ pair or a gg pairs or to the initial partons.

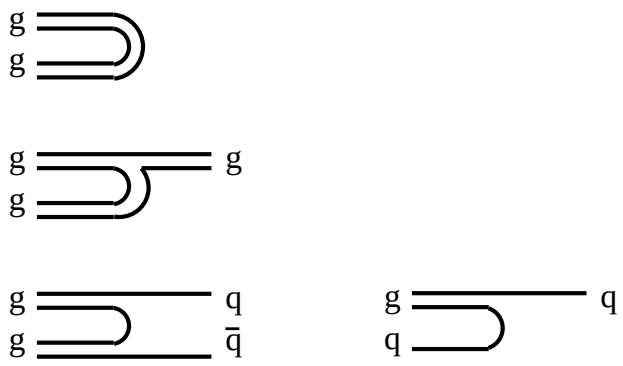

Figure 1: Color connection for gg (left) and gq (right).

3.4 Democratic Decay

We assume a democratic decay, constrained by the conservation laws. The number of degrees of freedom for each particle takes into account charge, spin and color. We do not consider gravitons in this study. The mass of the SM Higgs is set at 120 GeV. Events are produced where the types of particles are chosen randomly with the probabilities listed in Table 3 and are accepted only if conservation laws can be applied.

Table 3: Degrees of freedom and assigned probability in the generator for each particle.

Particle	Degrees of freedom	Assigned probability
g (gluon)	8	0.0690
W	6	0.0517
Z	3	0.0259
γ	2	0.0172
lepton (e, μ, τ)	4	0.0345
neutrino $(\nu_e, \nu_\mu, \nu_\tau)$	4	0.0345
quark (u, d, c, s, t, b)	12	0.1034
Higgs	1	0.0086
Graviton	5	0.0000

3.5 Performance

Figure 2 shows the differential cross sections, calculated from Eq. (1). Figures 3 show the shape of the mass distributions of generated black holes. The distributions shown start at $M_{\rm BH} > M_P$ although, as mentioned above, the validity of the model applies in the region $M_{\rm BH} \gg M_P$.

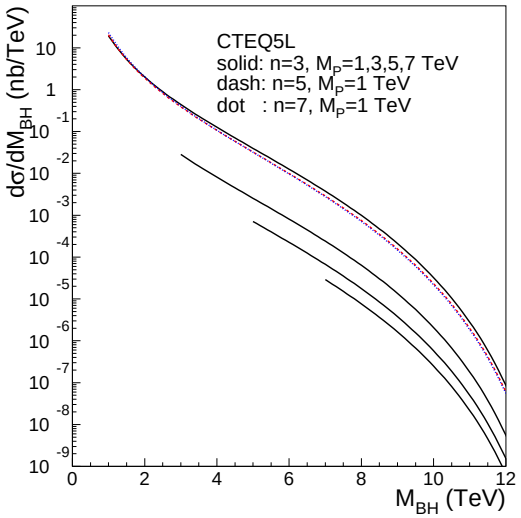

Figure 2: Differential cross section as a function of a black hole mass for each (M_P,n) parameter.

Figures 4 show various distributions of the generated black holes: p_z, charge, lepton number (L), baryon number (B), $B - L$, and the multiplicity of decay products. The absolute values of L are always even because of the spin conservation as shown at Figures 4 (c) and (g). When spin conservation is turned off, they take on both even and odd values, as shown at Figures 4 (h). Figures 4 (f),(i) and (j) indicate that the multiplicity of decay products depends on $M_{\rm BH}$ not M_P.

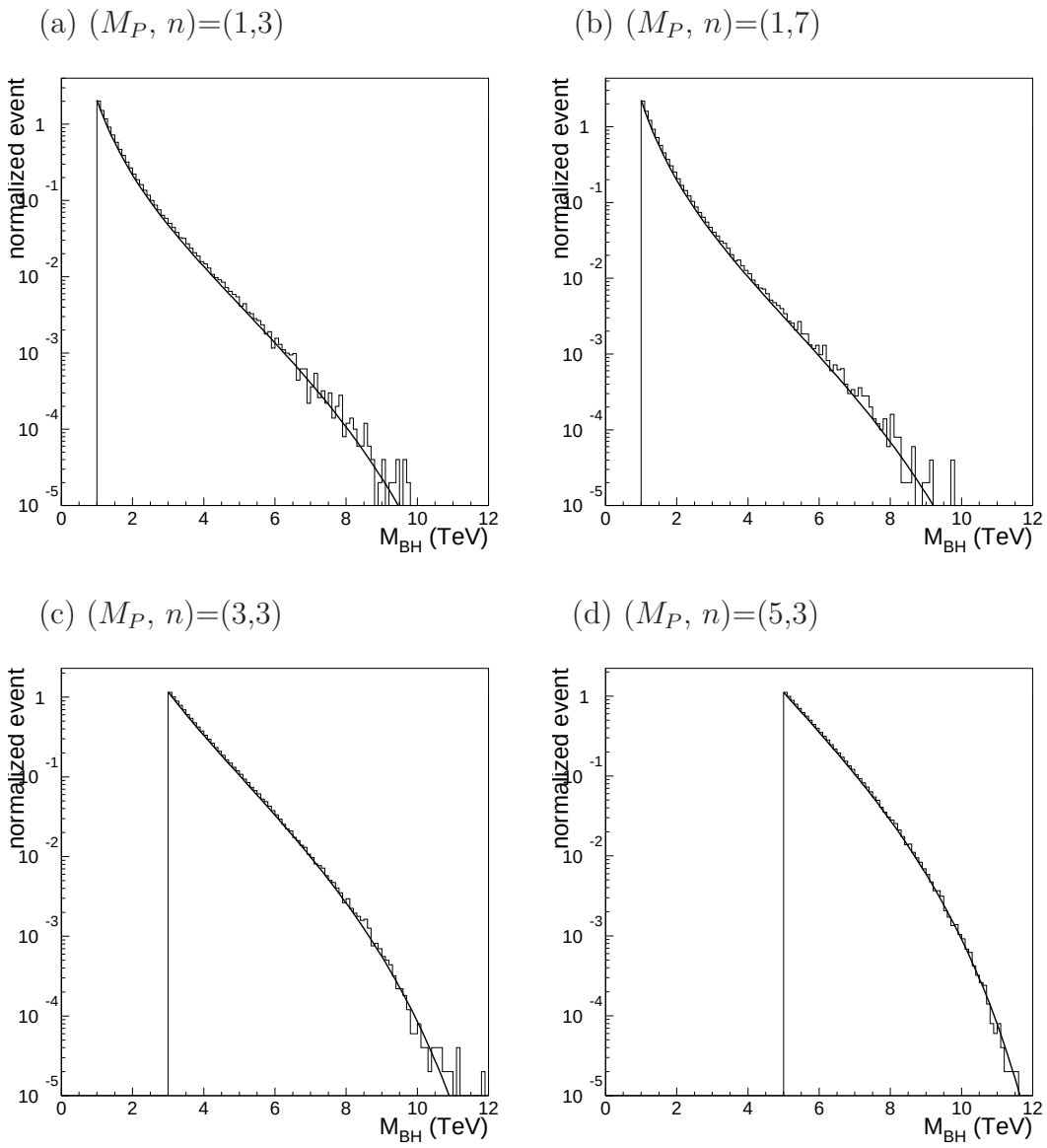

Figure 3: Mass distributions of the generated black holes. The histogram shows generated black holes and the solid line shows an expected shape from Eq. (1).

The distribution of particle types in the decay of black holes are shown in Figures 5. As expected, there are more quarks than anti-quarks (Figures 5 (a) and (b)) since the LHC is a proton-proton collider. We have also generated signal samples with (M_P, n, $f_{\rm BH}^{\rm th}$)=(1,3,9) in order to analyze events with high multiplicity of decay products. As the multiplicity of decay products becomes larger, the proportion of the different types of products becomes closer to the values of Table 3, even when many conservations are imposed, as can be seen shown in Figures 5 (c) and (d). When there is no charge and spin conservation, the ratios are almost the same as the values of Table 3, as shown at Figures 5 (e) and (f).

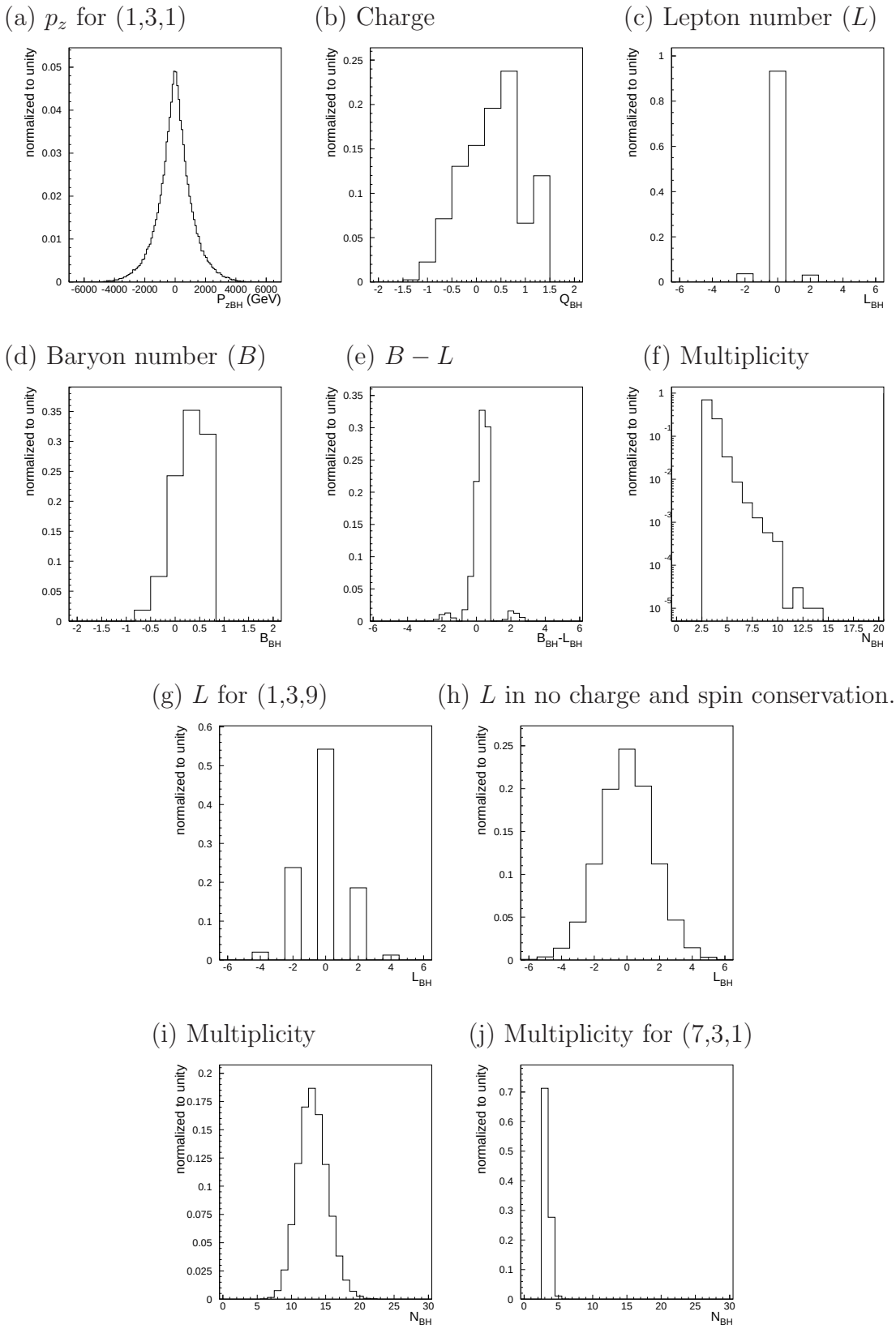

Figure 4: Distributions of generated black hole properties: p_z, charge, lepton number (L), baryon number (B), $B-L$, and multiplicity of decay products. (a)–(f) for (M_P, n, $f_{\rm BH}^{\rm th}$)=(1,3,1), (g)–(i) for (M_P, n, $f_{\rm BH}^{\rm th}$)=(1,3,9) and (j) for (M_P, n, $f_{\rm BH}^{\rm th}$)=(7,3,1).

(a) PDG code for (1,3,1)

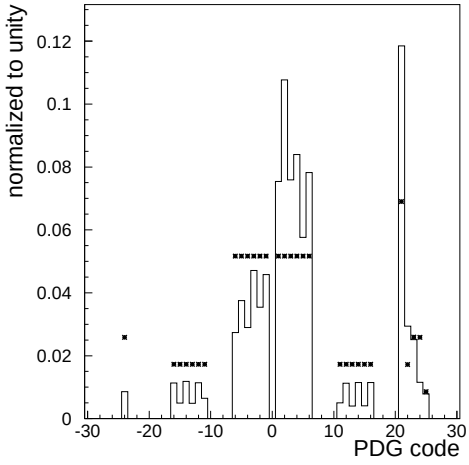

(b) |PDG code| for (1,3,1)

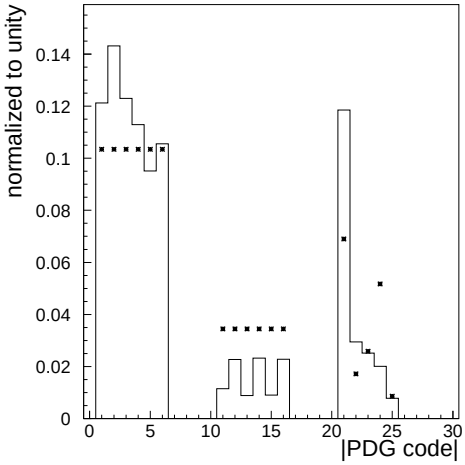

(c) PDG code for (1,3,9)

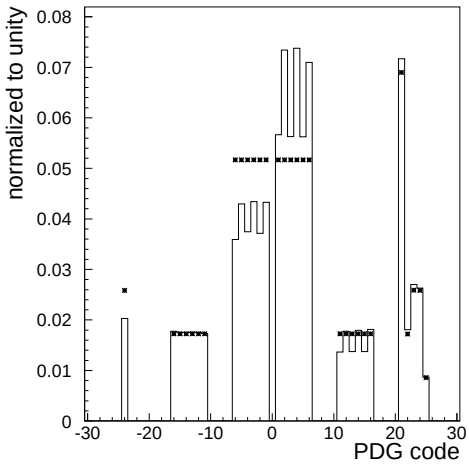

(d) |PDG code| for (1,3,9)

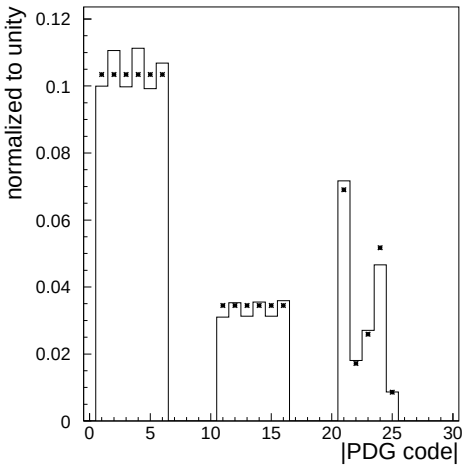

(e) PDG code for (1,3,9) in no charge and spin conservation.

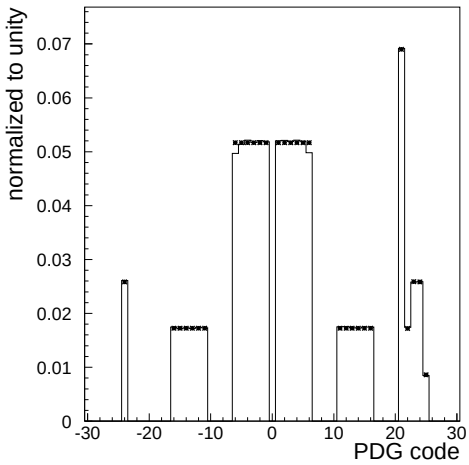

(f) |PDG code| for (1,3,9) in no charge and spin conservation.

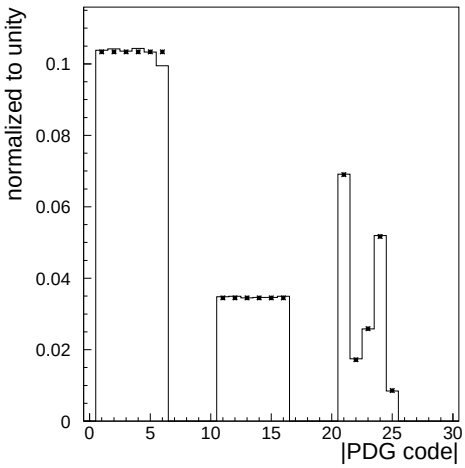

Figure 5: Distributions of PDG code of decay products of black holes. The left shows PDG code and the right shows absolute value of PDG code. The points of * show the values at Table 3.

Figures 6 show various distributions of the decay products: p_T, p_z, energy, η and ϕ. Distributions of p_z, η and ϕ of the products are symmetric as expected.

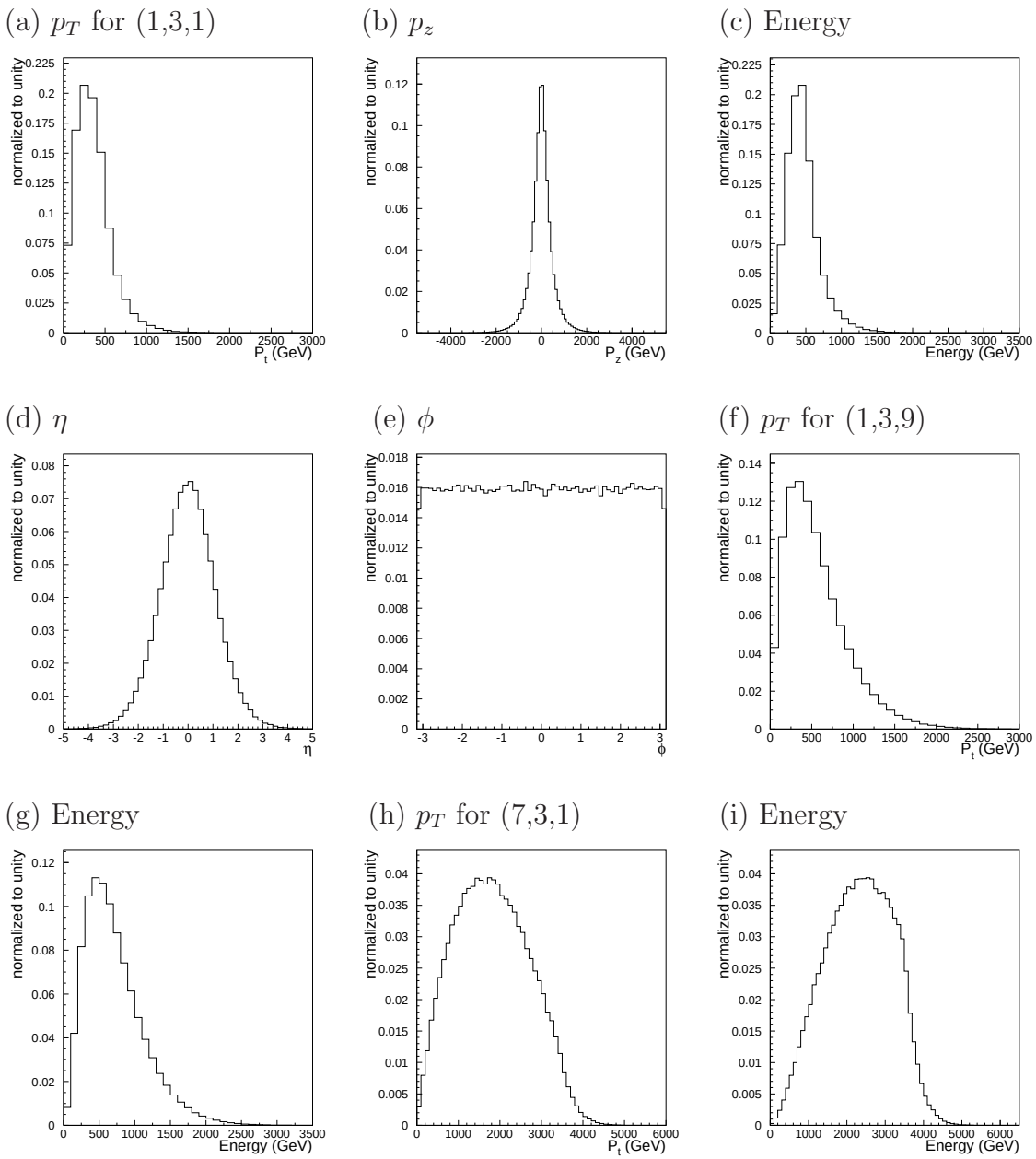

Figure 6: Distributions of various properties of decay products of black holes: p_T, p_z, energy, η and ϕ

4 Analysis

Although the expressions for black hole production given in Section 1 are not valid at $M_{\rm BH} \sim M_P$, our BH generator applies them in all the regions where $M_{\rm BH} > M_P$ in this study.

4.1 Selection Criteria and Reconstruction

The following cuts are applied in order to select and reconstruct black holes (BHs):

- For a precise reconstruction of the BH, it is necessary to remove particles produced in the stage of initial state radiations (ISRs). Because the particles from ISRs tend to have small p_T and large $|\eta|$, as shown in Figures. 7 and 8, the following requirements are applied to particles in each event (ISR-cut) :
  - $p_T > 30$ GeV for μ, e
  - $p_T > 50$ GeV for γ, jet

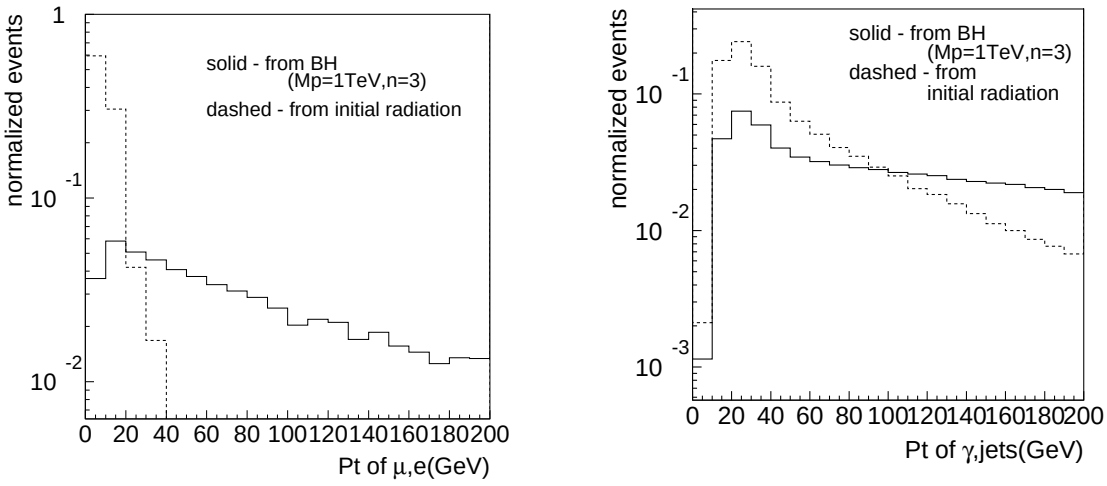

Figure 7: p_T distributions : comparison between particles from BH and initial state radiation ($M_P = 1$ TeV, n=3).

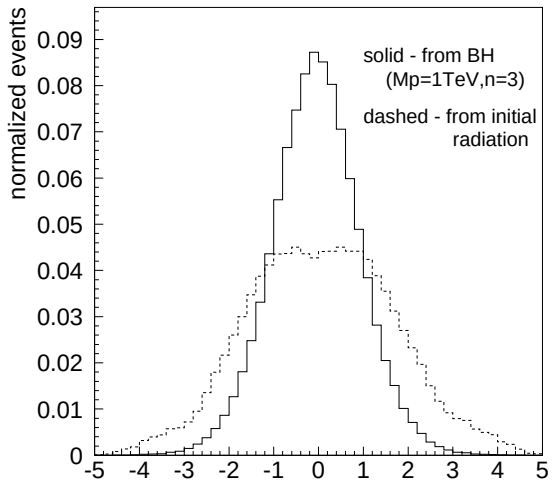

Figure 8: η distributions : comparison between particles from BH and initial state radiation ($M_P = 1$ TeV, n=3).

- Of all the particles passing the ISR-cut, more than three are required to have energy larger than 300 GeV ($E > 300$ GeV), and moreover, at least one of them has to be either an electron or a photon. This latter requirement is to suppress backgrounds. Figure 9 shows the distributions of the number of energetic particles in each event, where γq event is one of the largest contribution in the backgrounds as shown in Table 4. It is seen that this multiplicity cut on energetic particles is very effective.

- We require the event shape variable R_2 to be less than 0.8 ($R_2 < 0.8$). R_2 represents an event topology and it is defined by Fox-Wolfram moments as follows:

$$R_2 \equiv H_2/H_0$$

$$H_i \equiv \sum_{j,k} \frac{\mid p_j^* \mid\mid p_k^* \mid}{E^2} P_i(cos\phi_{jk})$$

  where H_i is the i-th Fox-Wolfram moments, j and k are ID numbers of tracks, p_j^* is the momentum of the track j in the rest frame of BH, ϕ_{jk} is the opening angle between the tracks j and k , and $P_i(x)$ is the Legendre polynomial. E is obtained by summing up the energies of particles passing the ISR-cut, calculated in the rest frame of BH. R_2 ranges from 0 to 1 ($0 \leq R_2 \leq 1$) as can be seen from Figure 10 which shows the R_2 distribution for signal and qq events with or without selection criteria. Since lower value of R_2 indicates more spherical event, we remove qq events here.

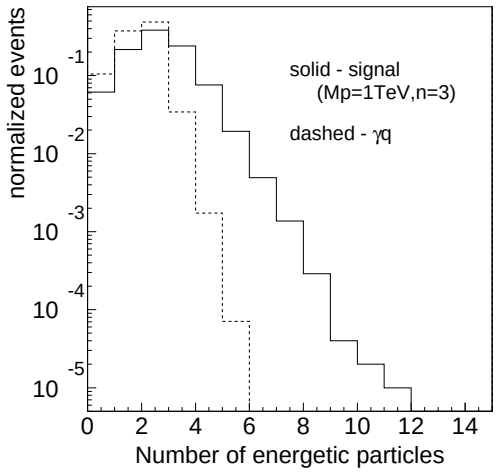

Figure 9: Shape of the distribution of the number of energetic particles with $E >$ 300 GeV : comparison between signal and γq background ($M_P = 1$ TeV, n=3).

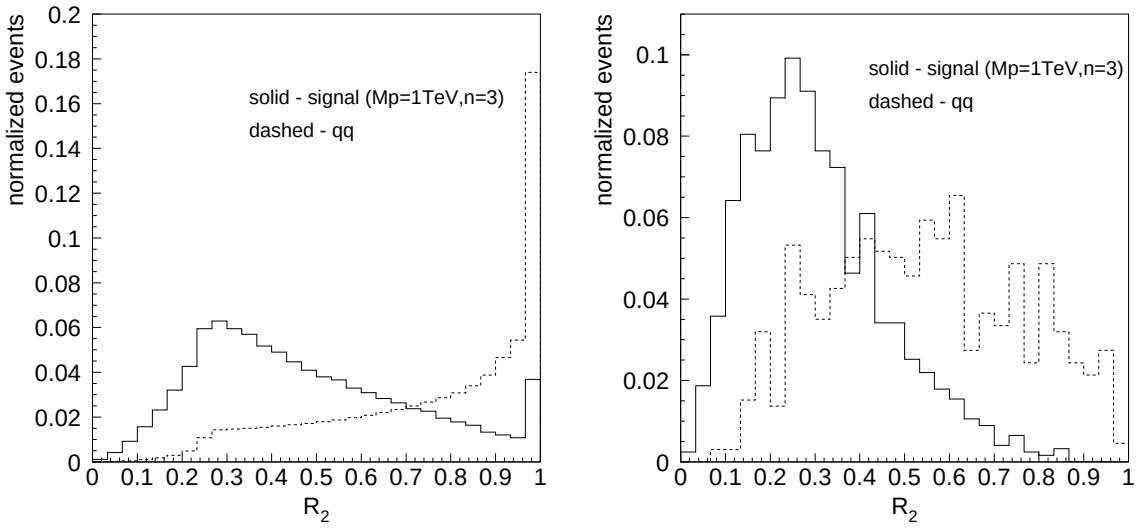

Figure 10: R_2 Distributions : comparison between signal event and qq event ($M_P = 1$ TeV, n=3). Left: without any selection criteria and right: with selection criteria

- $\not{E}_T < 100$ GeV. For a precise calculation of BH mass, events with high missing energy are rejected here.

The black hole mass is then reconstructed from the 4-momenta of the remaining muons, electrons, gammas and jets as follows:

$$p_{\rm BH} = \sum_{i=\mu,e,\gamma,jet} p_i$$

$$M_{\rm BH} = \sqrt{p_{\rm BH}^2},$$

where p_i is a reconstructed four-momentum of each particle.

The quality of the reconstructed mass of the BH is discussed in Appendix A.

4.2 Discovery Potential

We have evaluated the discovery potential for the following cases of (M_P ,n):

$$\begin{cases} M_P = 1, 3, 4, 5, 6, 7 \text{ TeV} \\ n = 2, 3, 5, 7 \end{cases}$$

by using the selection criteria described in Section 4.1. Because M_P is an unknown parameter, we cannot set the proper cut value for the lower limit of $M_{\rm BH}$. Therefore we consider various values as follows and evaluate $S/\sqrt{B}$ in each case:

$$M_{\rm BH} > M_{\rm BH}^{\rm min} = 1, 2, 3, 4, 5 \text{ TeV}.$$

The $M_{\rm BH}$ distributions are shown in Figure 11 for different values of M_P with $n = 3$. These are obtained after all the selection criteria have been applied. The histograms represent the sum of signals and backgrounds with the cross-hatched part showing only backgrounds. Note that $M_{\rm BH}^{\rm min}$ is set to 1 TeV for this figure.

(a) M_P=1 TeV

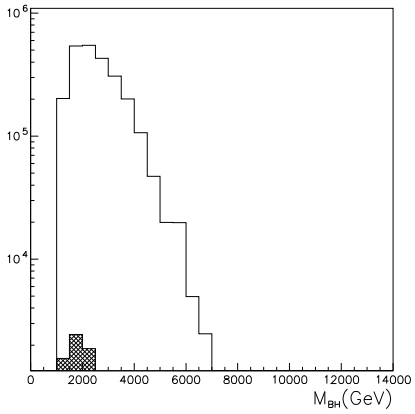

(b) M_P=3 TeV

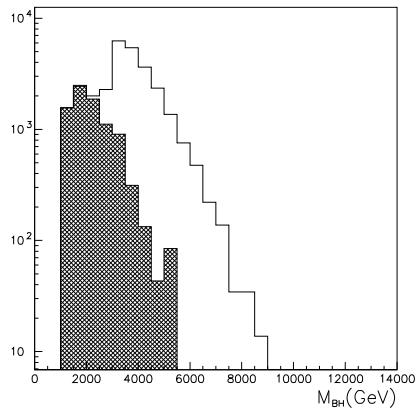

(c) M_P=4 TeV

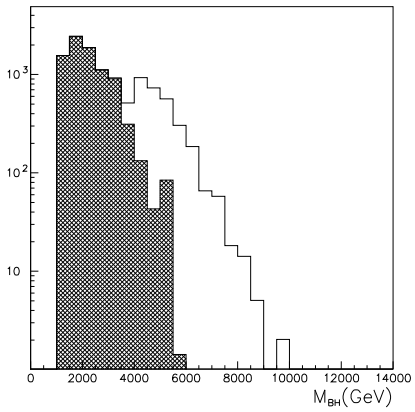

(d) M_P=5 TeV

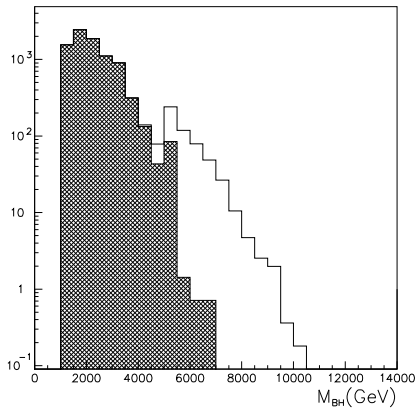

(e) M_P=6 TeV

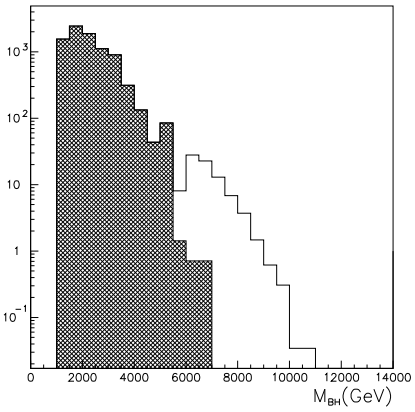

(f) M_P=7 TeV

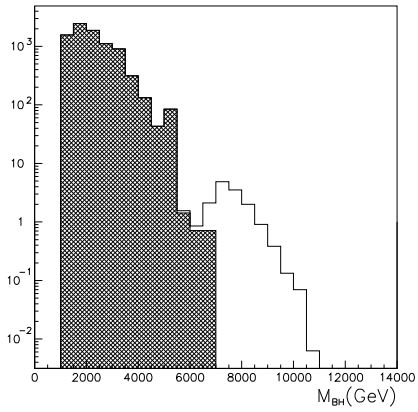

Figure 11: $M_{\rm BH}$ distributions in the case of n=3 and $M_{\rm BH}^{\rm min}$=1 TeV. (solid line : signal plus background, cross hatched : background only)

Table 4: The number of remaining BG events at $\int \mathcal{L}dt$=10 fb^{-1}. $\varepsilon^{M_{\rm BH}^{\rm min}=1}$ is the value of efficiency for $M_{\rm BH}^{\rm min} = 1$ TeV.

		qq	$\mathrm{t\bar{t}}$	$W^{\pm}W^{\mp}$
σ (pb)		$1.29 \cdot 10^4$	493	0.468
$\varepsilon^{M_{\rm BH}^{\rm min}=1}$		$1.67 \cdot 10^{-5}$	$1.39 \cdot 10^{-5}$	$8.5 \cdot 10^{-5}$
	1.0	$2.15 \cdot 10^3$	68.5	0.40
$M_{\rm BH}^{\rm min}$	2.0	$1.18 \cdot 10^3$	13	0.1
	3.0	$4.3 \cdot 10^2$	2	0.02
(TeV)	4.0	77	0.5	0
	5.0	$3 \cdot 10$	0	0

		$W^{\pm}Z$	ZZ	$\gamma\gamma$	γV
σ (pb)		25.9	10.6	229	280
$\varepsilon^{M_{\rm BH}^{\rm min}=1}$		$5 \cdot 10^{-7}$	$1.5 \cdot 10^{-6}$	0	$7 \cdot 10^{-7}$
	1.0	0.1	0.084	0	2
$M_{\rm BH}^{\rm min}$	2.0	0.05	0.04	0	1
	3.0	0	0	0	0
(TeV)	4.0	0	0	0	0
	5.0	0	0	0	0

		$W^{\pm}q$	Zq,γ^*q	γq	total
σ (pb)		73.4	31.5	23.5	
$\varepsilon^{M_{\rm BH}^{\rm min}=1}$		$4.7 \cdot 10^{-5}$	$1.40 \cdot 10^{-4}$	$1.484 \cdot 10^{-3}$	
	1.0	35	44.2	349.3	$2.66 \cdot 10^3$
$M_{\rm BH}^{\rm min}$	2.0	18	21	195	$1.43 \cdot 10^3$
	3.0	4	3.5	49.2	$4.9 \cdot 10^2$
(TeV)	4.0	0.7	0.3	7.8	86
	5.0	0	0	2.8	$3 \cdot 10$

Tables 4-6 show the number of events passing the selection criteria for background (BG) processes and signal events with various (M_P ,n). The number is normalized for $\int \mathcal{L}dt$=10 fb^{-1}. The values of efficiency are listed only for $M_{\rm BH}^{\rm min} = 1$ TeV. As can be seen in Table 4, γq process has the highest efficiency, but the background is dominated by the qq process owing to its large cross section. The total number of BG events is found to be $\sim 10^3$ - 10^4 in the case of $M_{\rm BH}^{\rm min} = 1$ - 2 TeV and ~ 10 - 10^2 in the case of $M_{\rm BH}^{\rm min} = 4$ - 5 TeV.

According to Tables 5 and 6, the efficiency for signal events is $\sim 1\%$ in all cases of (M_P ,n). It is relatively lower when $M_P = 1$ TeV or 7 TeV because signal events are more likely to be rejected by the $M_{\rm BH}^{\rm min}$ cut in the case of smaller M_P, or they have a large $\not{E}_T$ for larger M_P.

We calculate $S/\sqrt{B}$ from the data of Tables 4- 6 and estimate $\int \mathcal{L}_{\rm discovery}dt$ — the integrated luminosity with which discovery is achieved. Here the condition of discovery

Table 5: The number of remaining signal events at $\int \mathcal{L}dt$=10 fb^{-1}. $\varepsilon^{M_{\rm BH}^{\rm min}=1}$ is the value of efficiency for $M_{\rm BH}^{\rm min} = 1$ TeV.

(M_P, n)		(1,2)	(3,2)	(4,2)
σ (pb)		9450	25.51	3.738
$\varepsilon^{M_{\rm BH}^{\rm min}=1}$		9.63×10^{-3}	2.747×10^{-2}	2.733×10^{-2}
$M_{\rm BH}^{\rm min}$ (TeV)	1.0	9.10×10^5	7008	1022
	2.0	6.50×10^5	7002	1021
	3.0	2.52×10^5	6594	1016
	4.0	7.5×10^4	2987	943.5
	5.0	2.3×10^4	1.06×10^3	404.5

(M_P, n)		(5,2)	(6,2)	(7,2)
σ (pb)		0.6622	0.1249	2.292×10^{-2}
$\varepsilon^{M_{\rm BH}^{\rm min}=1}$		2.601×10^{-2}	2.287×10^{-2}	2.022×10^{-2}
$M_{\rm BH}^{\rm min}$ (TeV)	1.0	172.2	28.56	4.634
	2.0	172.2	28.54	4.634
	3.0	171.7	28.53	4.632
	4.0	170.1	28.46	4.616
	5.0	154.2	28.15	4.593

(M_P, n)		(1,3)	(3,3)	(4,3)
σ (pb)		8256	22.89	3.381
$\varepsilon^{M_{\rm BH}^{\rm min}=1}$		8.46×10^{-3}	2.725×10^{-2}	2.605×10^{-2}
$M_{\rm BH}^{\rm min}$ (TeV)	1.0	6.98×10^5	6238	880.8
	2.0	4.82×10^5	6224	879.4
	3.0	2.01×10^5	5878	874.0
	4.0	5.8×10^4	2745	810.8
	5.0	1.2×10^4	929	354.3

(M_P, n)		(5,3)	(6,3)	(7,3)
σ (pb)		0.6027	0.1142	2.105×10^{-2}
$\varepsilon^{M_{\rm BH}^{\rm min}=1}$		2.574×10^{-2}	2.347×10^{-2}	2.071×10^{-2}
$M_{\rm BH}^{\rm min}$ (TeV)	1.0	155.1	26.80	4.359
	2.0	155.1	26.80	4.357
	3.0	154.4	26.76	4.351
	4.0	152.7	26.59	4.341
	5.0	140.4	26.23	4.317

Table 6: The number of remaining signal events at $\int \mathcal{L}dt$=10 fb^{-1}. $\varepsilon^{M_{\rm BH}^{\rm min}=1}$ is the value of efficiency for $M_{\rm BH}^{\rm min} = 1$ TeV.

(M_P, n)		(1,5)	(3,5)	(4,5)
σ (pb)		8244	23.42	3.487
$\varepsilon^{M_{\rm BH}^{\rm min}=1}$		7.24×10^{-3}	2.563×10^{-2}	2.779×10^{-2}
$M_{\rm BH}^{\rm min}$ (TeV)	1.0	5.97×10^5	6003	969.0
	2.0	4.24×10^5	5993	969.0
	3.0	1.72×10^5	5600	964.5
	4.0	5.0×10^4	2497	892.0
	5.0	1.4×10^4	775	377.3

(M_P, n)		(5,5)	(6,5)	(7,5)
σ (pb)		0.6252	0.1191	2.203×10^{-2}
$\varepsilon^{M_{\rm BH}^{\rm min}=1}$		2.501×10^{-2}	2.244×10^{-2}	2.139×10^{-2}
$M_{\rm BH}^{\rm min}$ (TeV)	1.0	156.4	26.73	4.712
	2.0	156.3	26.73	4.712
	3.0	155.7	26.69	4.706
	4.0	154.9	26.61	4.688
	5.0	139.2	26.33	4.662

(M_P, n)		(1,7)	(3,7)	(4,7)
σ (pb)		9053	26.02	3.887
$\varepsilon^{M_{\rm BH}^{\rm min}=1}$		6.54×10^{-3}	2.577×10^{-2}	2.630×10^{-2}
$M_{\rm BH}^{\rm min}$ (TeV)	1.0	5.92×10^5	6705	1022
	2.0	4.22×10^5	6698	1020
	3.0	1.57×10^5	6310	1017
	4.0	4.5×10^4	2789	943.0
	5.0	5×10^3	892	382

(M_P, n)		(5,7)	(6,7)	(7,7)
σ (pb)		0.6991	0.1335	2.474×10^{-2}
$\varepsilon^{M_{\rm BH}^{\rm min}=1}$		2.577×10^{-2}	2.319×10^{-2}	2.090×10^{-2}
$M_{\rm BH}^{\rm min}$ (TeV)	1.0	180.2	30.96	5.171
	2.0	180.2	30.93	5.171
	3.0	179.7	30.89	5.168
	4.0	178.3	30.72	5.151
	5.0	164.7	30.48	5.124

Table 7: The value of $S/\sqrt{B}$ at $\int \mathcal{L}dt$=10 fb^{-1}.

(M_P, n)		(1,2)	(3,2)	(4,2)
σ (pb)		9450	25.51	3.738
$M_{\rm BH}^{\rm min}$ (TeV)	1.0	1.76×10^4	136	19.8
	2.0	1.72×10^4	185	27.0
	3.0	1.1×10^4	3.0×10^2	46
	4.0	8.1×10^3	3.2×10^2	1.0×10^2
	5.0	4×10^3	2×10^2	7×10

(M_P, n)		(5,2)	(6,2)	(7,2)
σ (pb)		0.6622	0.1249	2.292×10^{-2}
$M_{\rm BH}^{\rm min}$ (TeV)	1.0	3.34	0.554	0.0899
	2.0	4.55	0.755	0.123
	3.0	7.8	1.3	0.21
	4.0	18	3.1	0.50
	5.0	3×10	5	0.8

(M_P, n)		(1,3)	(3,3)	(4,3)
σ (pb)		8256	22.89	3.381
$M_{\rm BH}^{\rm min}$ (TeV)	1.0	1.35×10^4	121	17.1
	2.0	1.27×10^4	165	23.3
	3.0	9.1×10^3	2.7×10^2	39
	4.0	6.3×10^3	3.0×10^2	87
	5.0	2×10^3	2×10^2	6×10

(M_P, n)		(5,3)	(6,3)	(7,3)
σ (pb)		0.6027	0.1142	2.105×10^{-2}
$M_{\rm BH}^{\rm min}$ (TeV)	1.0	3.01	0.520	0.0845
	2.0	4.10	0.709	0.115
	3.0	7.0	1.2	0.20
	4.0	16	2.9	0.47
	5.0	3×10	5	0.8

Table 8: The value of $S/\sqrt{B}$ at $\int \mathcal{L}dt$=10 fb^{-1}.

(M_P, n)		(1,5)	(3,5)	(4,5)
σ (pb)		8244	23.42	3.487
$M_{\rm BH}^{\rm min}$ (TeV)	1.0	1.16×10^4	116	18.8
	2.0	1.12×10^4	158	25.6
	3.0	7.8×10^3	2.5×10^2	44
	4.0	5.4×10^3	2.7×10^2	96
	5.0	3×10^3	1×10^2	7×10

(M_P, n)		(5,5)	(6,5)	(7,5)
σ (pb)		0.6252	0.1191	2.203×10^{-2}
$M_{\rm BH}^{\rm min}$ (TeV)	1.0	3.03	0.518	0.0914
	2.0	4.13	0.707	0.125
	3.0	7.0	1.2	0.21
	4.0	17	2.9	0.51
	5.0	3×10	5	0.9

(M_P, n)		(1,7)	(3,7)	(4,7)
σ (pb)		9053	26.02	3.887
$M_{\rm BH}^{\rm min}$ (TeV)	1.0	1.15×10^4	130	19.8
	2.0	1.11×10^4	177	27.0
	3.0	7.1×10^3	2.9×10^2	46
	4.0	4.9×10^3	3.0×10^2	1.0×10^2
	5.0	9×10^2	2×10^2	7×10

(M_P, n)		(5,7)	(6,7)	(7,7)
σ (pb)		0.6991	0.1335	2.474×10^{-2}
$M_{\rm BH}^{\rm min}$ (TeV)	1.0	3.49	0.600	0.100
	2.0	4.77	0.818	0.137
	3.0	8.1	1.4	0.23
	4.0	19	3.3	0.56
	5.0	3×10	6	0.9

is set as:

$$S/\sqrt{B} \ \geq \ 5.0 \qquad \text{and} \qquad S \ \geq \ 10$$

which is a conventional condition, as used in the analysis of Higgs events with ATLAS. The results for $S/\sqrt{B}$ and $\int \mathcal{L}_{\rm discovery} dt$ are shown in Table 7-8 and 9 respectively. We require that $M_{\rm BH}^{\rm min}$ be larger than M_P to calculate integrated luminosities for BH discovery. In Table 9, the shaded values indicate the most favorable cut in $M_{\rm BH}^{\rm min}$ in each case of (M_P ,n). From these tables, we see that the discovery can be accomplished within $\int \mathcal{L}_{\rm discovery} dt \leq$ 1 fb^{-1} in all cases of n if M_P is less than $\sim$ 5 TeV.

Figure 12 gives a contour plot for $\int \mathcal{L}_{\rm discovery} dt$ in (M_P ,n) plane. We find that the discovery potential hardly depends on n but has a strong dependence on M_P. This is due to the fact that the cross section is a strong function of M_P but not of n, as shown in Tables 5 and 6. From this relation between M_P and $\int \mathcal{L}_{\rm discovery} dt$, M_P can be determined by how early the discovery is accomplished.

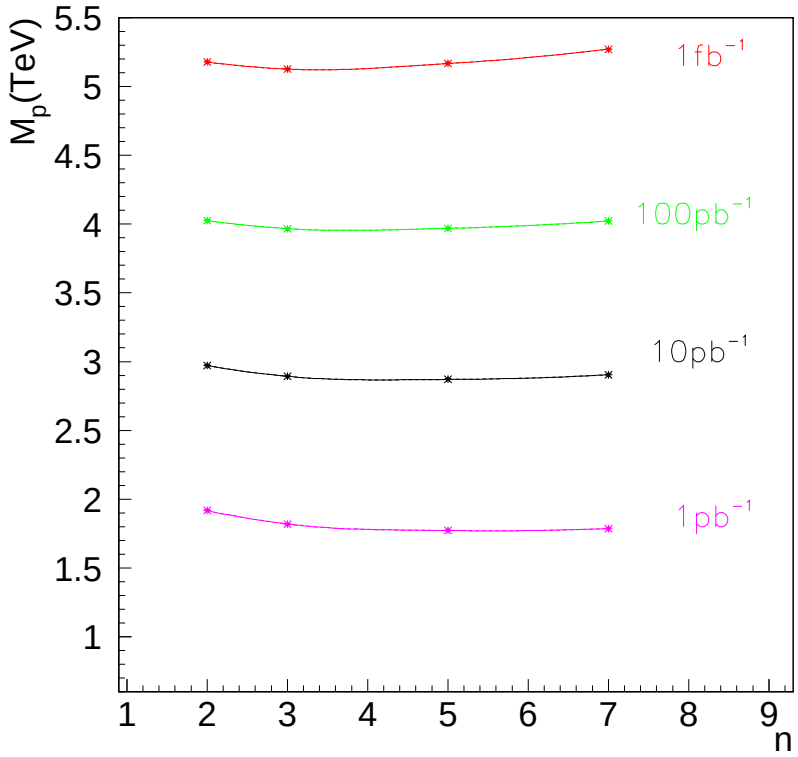

Figure 12: Contours of $\int \mathcal{L}_{\rm discovery} dt$ in (M_P, n) plane.

In a quantitative point of view, it is found that the excess of events is detected in $\sim$ 1 month at low luminosity ($\int \mathcal{L}dt$=1 fb^{-1}) if $M_P < 5$ TeV, and discovery within only one day ($\int \mathcal{L}dt$=100 pb^{-1}) can be expected if $M_P < 4$ TeV.

As was previously mentioned, the BH model we assumed here is valid only when $M_{\rm BH} \gg M_P$. As $M_{\rm BH}$ approaches M_P, the theory of BH production becomes very complex. If we consider events with reconstructed $M_{\rm BH} > 5$ TeV in the case of $M_P =$

Table 9: Integrated luminosity (fb^{-1}) required for discovery, for various values of (M_P, n), as a function of $M_{\rm BH}^{\rm min}$ ($M_{\rm BH}^{\rm min} \geq M_P$). The shaded entry gives the most favorable value in each case of (M_P, n).

(M_P, n)		(1,2)	(3,2)	(4,2)	(5,2)
σ (pb)		9450	25.51	3.738	0.6622
$M_{\rm BH}^{\rm min}$ (TeV)	1.0	1.10×10^{-4}	-	-	-
	2.0	1.54×10^{-4}	-	-	-
	3.0	3.97×10^{-4}	1.517×10^{-2}	-	-
	4.0	1.3×10^{-3}	3.348×10^{-2}	0.1060	-
	5.0	4.3×10^{-3}	9.43×10^{-2}	0.2472	0.6485

(M_P, n)		(1,3)	(3,3)	(4,3)	(5,3)
σ (pb)		8256	22.89	3.381	0.6027
$M_{\rm BH}^{\rm min}$ (TeV)	1.0	1.43×10^{-4}	-	-	-
	2.0	2.07×10^{-4}	-	-	-
	3.0	4.98×10^{-4}	1.701×10^{-2}	-	-
	4.0	1.7×10^{-3}	3.643×10^{-2}	0.1233	-
	5.0	8.3×10^{-3}	0.108	0.2822	0.7123

(M_P, n)		(1,5)	(3,5)	(4,5)	(5,5)
σ (pb)		8244	23.42	3.487	0.6252
$M_{\rm BH}^{\rm min}$ (TeV)	1.0	1.68×10^{-4}	-	-	-
	2.0	2.36×10^{-4}	-	-	-
	3.0	5.81×10^{-4}	1.786×10^{-2}	-	-
	4.0	2.0×10^{-3}	4.005×10^{-2}	0.1121	-
	5.0	7.1×10^{-3}	0.129	0.2650	0.7184

(M_P, n)		(1,7)	(3,7)	(4,7)	(5,7)
σ (pb)		9053	26.02	3.887	0.6991
$M_{\rm BH}^{\rm min}$ (TeV)	1.0	1.69×10^{-4}	-	-	-
	2.0	2.37×10^{-4}	-	-	-
	3.0	6.37×10^{-4}	1.585×10^{-2}	-	-
	4.0	2.2×10^{-3}	3.586×10^{-2}	0.1060	-
	5.0	2×10^{-2}	0.112	0.262	0.6072

1 TeV, we find that we need $\sim$5 pb^{-1} instead of $\sim$0.1 pb^{-1} to discover black holes. However the events include black holes whose generated mass was less then 5 TeV. When black holes with mass greater than 5 TeV are generated, we find that we need $\sim$10 pb^{-1}.

Considering that the model of BH formation and decay is valid only for $M_{\rm BH} \gg M_P$, we show, in Figure 13, an evaluation of the discovery potential of BHs when the cut $M_{\rm BH}^{\rm min} > M_P + 1$ TeV is applied. Although more integrated luminosity is required, it is clear that an excess of events will still be easily observed within a few days of running, for M_P values up to a few TeV.

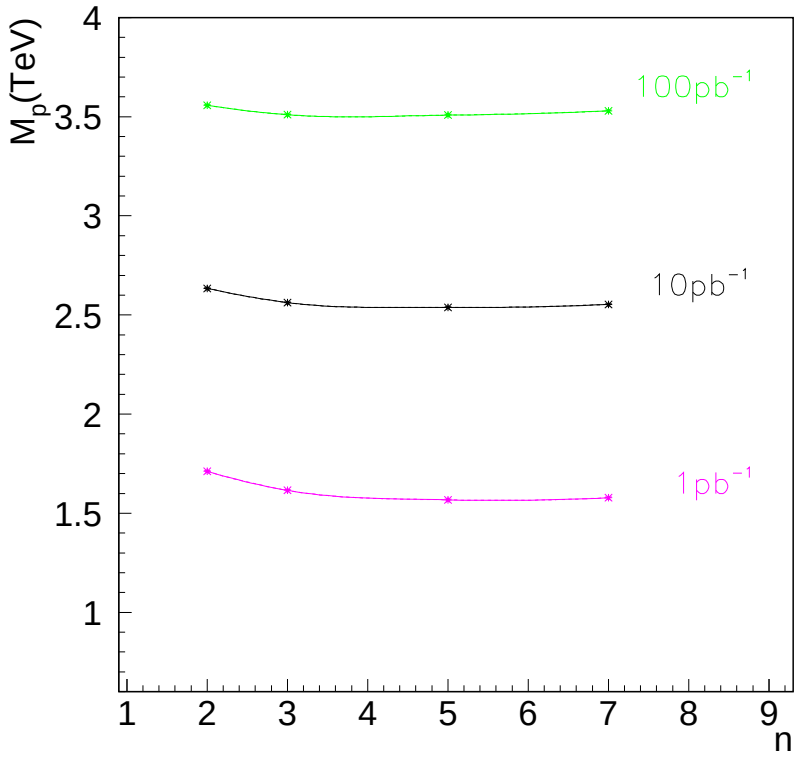

Figure 13: Contours of $\int \mathcal{L}_{\rm discovery} dt$ in $(M_P,\, n)$ plane in case of $M_{\rm BH}^{\rm min} > M_P + 1$ TeV.

5 Conclusion

We have studied the potential to observe black holes with the ATLAS detector at the LHC. We developed a generator of black holes with simple assumptions for the production and decay process, taking the expressions in Section 1 as valid in the full region of the black hole mass $M_{\rm BH} > M_P$. We find an excess of events from the Standard Model backgrounds for the integrated luminosity of 1 fb^{-1} ($\sim$ 1 month at low luminosity) if $M_P < 5$ TeV and with the integrated luminosity of 100 pb^{-1} ($\sim$ 1 day) if $M_P < 4$ TeV. If we assume validity when $M_{\rm BH} > M_P + 1$ TeV, the required luminosities are slightly larger.

We also proposed a simple method to estimate the Planck scale M_P. It will be necessary to find a way to estimate the number of large extra dimensions n and to identify the excess as the black holes. The development of more realistic black hole generators is also important for more detail studies.

Acknowledgments

We thank to G. Azuelos and L. Poggioli for thier suggestions for our analysis.

A Reconstructed Mass of Black Hole

The resolution in the reconstructed mass of the BH depends on various factors. We investigate reasons of the overestimation and the underestimation on the reconstructed mass $M_{\rm BH}$ as follows.

Figures 14 show distributions of $M_{\rm BH} - M_{\rm BH}^{\rm true}$ for BH events with $M_{\rm BH}^{\rm true} \geq 1.0, 6.0,$ and 9.0 TeV in case of $(M_P, n) = (1,3)$, respectively.

(a) (M_P, n, $f_{\rm BH}^{\rm th}$)=(1,3,1) (b) (M_P, n, $f_{\rm BH}^{\rm th}$)=(1,3,6) (c) (M_P, n, $f_{\rm BH}^{\rm th}$)=(1,3,9)

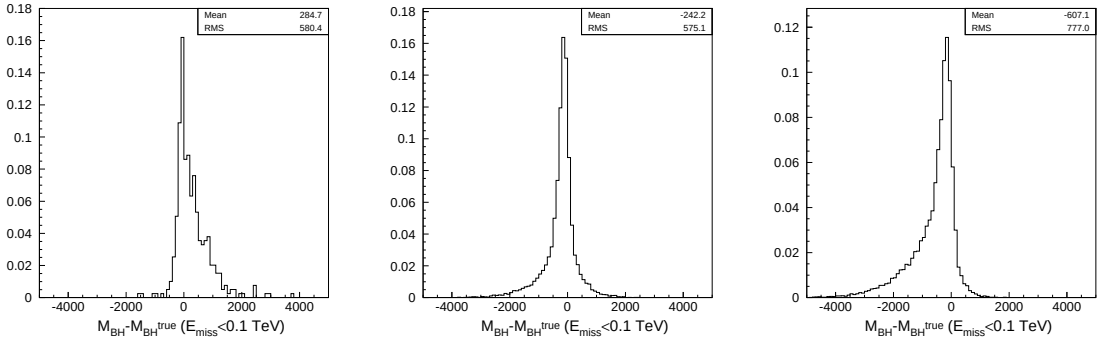

Figure 14: Distributions of the difference between a reconstructed and a generated mass of a black hole $M_{\rm BH} - M_{\rm BH}^{\rm true}$. Our selection criteria is applied to reconstruct a black hole. E_{miss} in the figure means $\not{E}_T$.

There are contaminations from particles arising from the initial state radiation and from the spectator proton fragments of the hard scattering. We call these particles "ISRs/SPECs". Figures 15 show $M_{\rm BH} - M_{\rm BH}^{\rm true}$ distributions of the events with no neutrino. We compare the difference in mass when all particles are used and when ISRs/SPECs are excluded. The generator information is used to determine whether a particle comes from ISRs/SPECs. We can see that the overestimation of a black hole mass is due to the contaminations of ISRs/SPECs.

(a) $(M_P,\, n,\, f_{\rm BH}^{\rm th})$=(1,3,1) (b) $(M_P,\, n,\, f_{\rm BH}^{\rm th})$=(1,3,6) (c) $(M_P,\, n,\, f_{\rm BH}^{\rm th})$=(1,3,9)

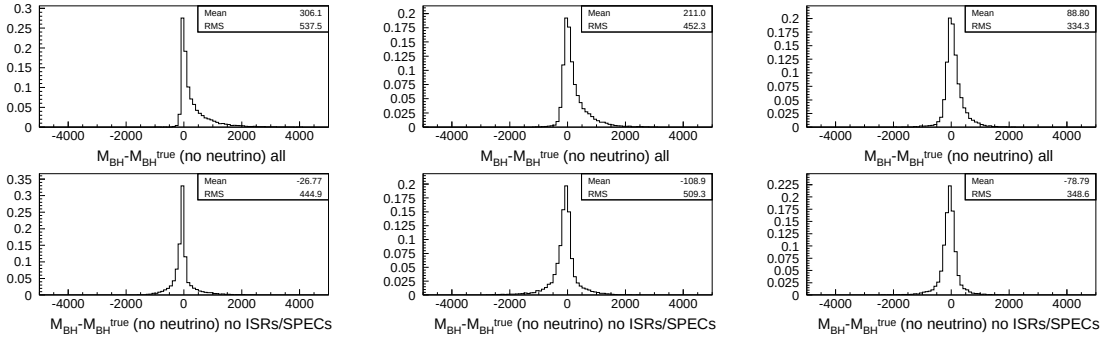

Figure 15: $M_{\rm BH} - M_{\rm BH}^{\rm true}$ Distributions. We use events with no neutrino. The upper figure is obtained from all reconstructed particles and jets and the lower is from them except for ISRs/SPECs. Details are given in the text.

Figure 16 shows the correlation between a $M_{\rm BH} - M_{\rm BH}^{\rm true}$ and a measured missing energy $\not{E}_T$. We can see clearly that we underestimate a black hole mass if the missing energy is important.

(a) $(M_P,\, n,\, f_{\rm BH}^{\rm th})$=(1,3,1) (b) $(M_P,\, n,\, f_{\rm BH}^{\rm th})$=(1,3,6) (c) $(M_P,\, n,\, f_{\rm BH}^{\rm th})$=(1,3,9)

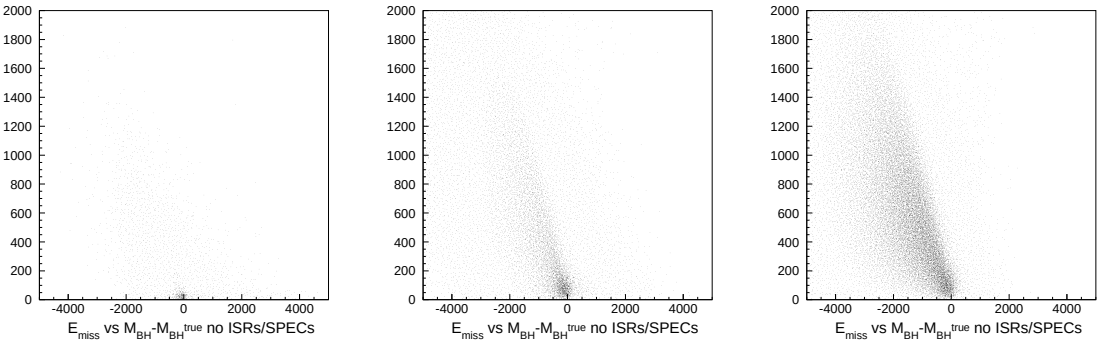

Figure 16: Measured missing energy $\not{E}_T$ versus $M_{\rm BH} - M_{\rm BH}^{\rm true}$. The mass of a black hole is obtained from reconstructed particles and jets except for ISRs/SPECs.

We perform various corrections:(1) we subtract the momentum of particles which are selected by our criteria but come from ISRs/SPECs, from the reconstructed mass $M_{\rm BH}$, (2) add the momentum of neutrinos, (3) add the momentum of particles which do not come from ISRs/SPECs but are removed by our selection criteria, as shown at Figures 17. We can see that the reconstructed mass is improved by these corrections as we expected. From these results we understand that the overestimation of $M_{\rm BH}$ is caused by the contamination of particles from the initial state radiation and the spectators while the underestimation is due to the missing energy of neutrinos.

(a) (M_P, n, $f_{\rm BH}^{\rm th}$)=(1,3,1) (b) (M_P, n, $f_{\rm BH}^{\rm th}$)=(1,3,6) (c) (M_P, n, $f_{\rm BH}^{\rm th}$)=(1,3,9)

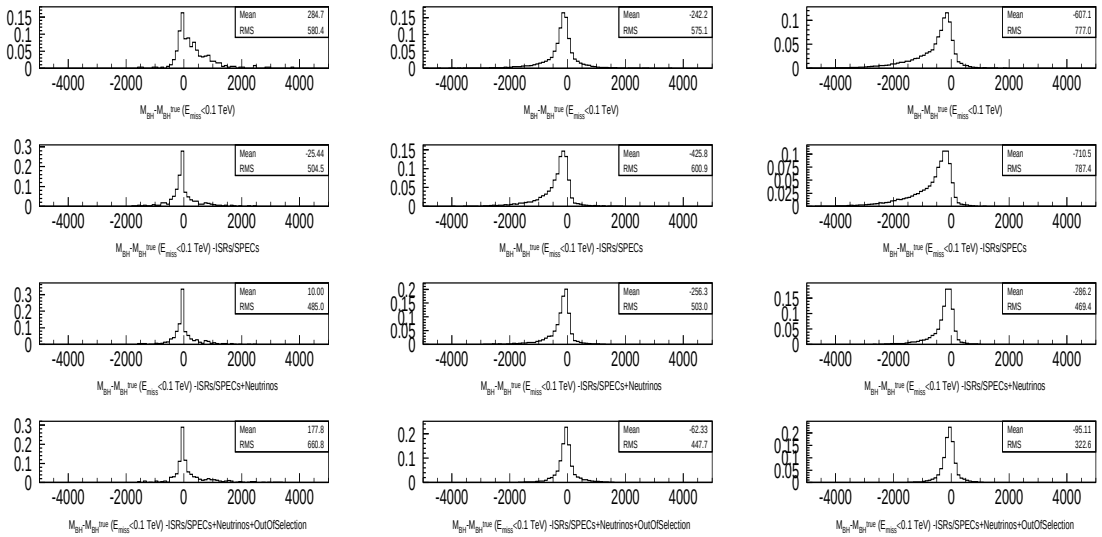

Figure 17: $M_{\rm BH} - M_{\rm BH}^{\rm true}$ Distributions. The top figures are the same with Figures 14. The 2nd, 3rd and bottom figures show $M_{\rm BH} - M_{\rm BH}^{\rm true}$ distributions corrected step-by-step. Details are given in the text.

References

[1] S. Dimopoulous and G. Landsberg Phys. Rev. Lett. **87**, 161602 (2001)

[2] S. B. Giddings and S. Thomas Phys. Rev. D **65**, 056010 (2002)

[3] N. Arkani-Hamed, S. Dimopoulous, and G. Dvali Phys. Lett. B **429**, 263 (1998)

[4] J. Chiaverini, S. J. Smullin, A. A. Geraci, D. M. Weld and A. Kapitulnik Phys. Rev. Lett. **90**, 151101 (2003)

[5] Particle Data Group, K. Hagiwara *et al.*, Phys. Rev. D **66**, 010001 (2002)

[6] Y. Uehara Mod. Phys. Lett. A **17** 1551 (2002)

[7] M. B. Voloshin Phys. Lett. B **518**, 137 (2001), M. B. Voloshin Phys. Lett. B **524**, 376 (2002)

[8] D. M. Eardley and S. B. Giddings Phys. Rev. D **66**, 044011 (2002), H. Yoshino and Y. Nambu Phys. Rev. D **66**, 065004 (2002), H. Yoshino and Y. Nambu Phys. Rev. D **67**, 024009 (2003), S. N. Solodukhin Phys. Lett. B **533**, 153 (2002), S. D. H. Hsu Phys. Lett. B **555**, 92 (2003)

[9] T. Sjostrand *et al.* hep-ph/018264. PYTHIA 6.206 is used for the signal and 6.203 for the background.

[10] E. Richter-Was, D. Froidevaux, and L. Poggioli, ATLAS internal note ATL-PHYS-98-131 (1998).

[11] G. Landsberg, SUSY 2002 Conference, DESY, Hamburg, June 17-23, 2002, hep-ph/0211043

[12] The other black hole generator, CHARYBDIS, has been developed, which takes into account more realistic effects. See C. M. Harris, P. Richardson and B. R. Webber hep-ph/0307305.